

PAPER

Energetics, migration and trapping of Zn interstitials in ZnO

To cite this article: Alexander Azarov and Andrej Kuznetsov 2019 *J. Phys. D: Appl. Phys.* **52** 485103

View the [article online](#) for updates and enhancements.

You may also like

- [Effect of Post-Annealing on Structural and Electrical Properties of ZnO:In Films](#)
Guo-Ping Qin, , Hong Zhang et al.
- [Investigation of \$V_{\text{O}}\$ -Zn native donor complex in MBE grown bulk ZnO](#)
M Asghar, K Mahmood, I T Ferguson et al.
- [Structural, optical, and antibacterial properties of Li-doped ZnO nanoparticles synthesized in water: evidence of incorporation of interstitial Li](#)
Sumit Mukherjee, Subhamay Pramanik, Sandip Das et al.

Energetics, migration and trapping of Zn interstitials in ZnO

Alexander Azarov^{1,2}  and Andrej Kuznetsov²

¹ NOMATEN Centre of Excellence, National Centre for Nuclear Research, A. Soltana 7, 05-400 Otwock-Świerk, Poland

² Department of Physics, Centre for Materials Science and Nanotechnology, University of Oslo, PO Box 1048 Blindern, N-0316 Oslo, Norway

E-mail: alexander.azarov@smn.uio.no

Received 15 July 2019, revised 15 August 2019

Accepted for publication 27 August 2019

Published 12 September 2019



Abstract

Zn interstitial (Zn_i) is one of the fundamental intrinsic defects in ZnO and prominently affects the physical properties of the material. Here, the energetics and migration properties of Zn_i have been studied in ion implanted ZnO using a new approach based on the Li marker diffusion. Specifically, ZnO single crystals were implanted with 3.2 keV/amu B and BF_2 ions and the release of Zn_i from the implanted regions during annealing was correlated with the advance of the characteristic Li depleted region into the bulk of the samples. Using this methodology, we calculate the activation energy of 1.45 eV to govern the process for B implants. Assuming that the migration energy of Zn_i to be of ~ 0.6 eV, as discussed previously in literature, a barrier for releasing Zn_i from the implanted region may be estimated as ~ 0.8 – 0.9 eV. Meanwhile, in the BF_2 implanted samples, the migration of Zn_i is less efficient, as interpreted from the Li redistribution features in these samples; in particular, it is argued that Zn_i may be trapped by defect complexes related to the presence of F.

Keywords: ZnO, interstitials, diffusion, radiation defects

(Some figures may appear in colour only in the online journal)

1. Introduction

Point defects and defect complexes affect practically all physical properties of solids. This holds also for ZnO which is a wide and direct band gap semiconductor having numerous potential applications in electronics, photonics, spintronics, sensors technologies, etc [1–3]. One of the major issues hindering the realization of ZnO bipolar devices is its native n-type conductivity and associated doping asymmetry, meaning that p-type doping is difficult to reach. Although the origin of the doping asymmetry is still not fully understood, it has been suggested that a spontaneous generation of the intrinsic defects (such as zinc interstitials (Zn_i) and oxygen vacancies (V_O)) in response to the Fermi level shifts and the formation of donor-like dopant-defect complexes can play a prominent role [4–7]. Nevertheless during the past decade a number of attempts have been performed to demonstrate p-type conductivity in ZnO using in-situ doping during synthesis, in-diffusion and/or ion implantation [8–11]. However,

the reliability of the p-type doping in ZnO is still limited and there is a room for improvements. Moreover, so-called self-compensation in heavily n-type doped material (due to formation of the acceptor-like defect complexes involving Zn vacancies (V_{Zn}) [12]) is a serious obstacle for the realization of n-type highly conductive transparent ZnO films, otherwise highly desirable for transparent electronics, solar cells, etc. Thus, understanding the mechanisms of the point defect formation and the evolution of their properties is both of fundamental interest and also crucial for the progress in realization of ZnO-based devices.

It should be noted that V_{Zn} energetics in ZnO can be revealed by analyzing Zn self-diffusion in isotopic heterostructures assuming V_{Zn} assisted mechanism for Zn transport [13, 14]. On the other hand, Zn_i remains invisible in such experiments. Indeed, despite that the migration energy of Zn_i was predicted to be low (e.g. ~ 0.6 eV in accordance with [15]), the formation energy maybe quite high [15]. Meanwhile, in experimental conditions Zn_i may be readily generated by ion implantation.

However, assuming the aim is to measure Zn_i migration, the remaining question is: what defect level or reaction is appropriate to monitor in order to relate it to the Zn_i diffusion mechanism. By far, two major approaches were discussed in literature. One approach relies on the low temperature implants and in-situ anneals, while measuring the evolution of the defect related signatures/processes, e.g. recovery of the carrier compensation [16], electron paramagnetic resonance [17], etc. The basic principle is straightforward—the decrease in the feature amplitude is correlated directly with the migration of the primary defects otherwise ‘frozen’ in the lattice by low temperature implants. Still, a significant weakness here is associated with an uncertainty of what kind of primary defects is actually responsible for the observation; and it specifically holds for compound semiconductors. For instance, for ZnO, it was argued that the migration of either Zn_i or oxygen interstitials (O_i) may be responsible for the carrier recovery first-order kinetics as observed in [16].

Another approach relies on the interpretations of the impurity diffusion assisted by self-interstitials. This approach is generic and was used to study self-interstitials in different semiconductors, for example, in Si investigating boron diffusion [18]. Specifically for ZnO it is possible to discriminate between Zn_i and O_i assisted process using appropriate diffusion marker. Indeed, it has been shown previously that the interaction of the radiation defects and implanted species with residual impurities, such as Li, can be used for investigations of Zn_i in ion implanted ZnO [19]. It should be noted that Li behavior in the ion implanted material is of interest by itself. Similar to other group-Ia impurities, Li residing on a Zn site (Li_{Zn}) is considered as a potential acceptor and Li p -type doping possibilities were investigated too (see, e.g. [20, 21]). However, despite a high Li solubility [22] the realization of stable p -type is hindered by the amphoteric nature of Li in ZnO [23]. Indeed, Li in its interstitial configuration (Li_i) exhibits donor behavior and Li_i formation energy dramatically decreases with lowering Fermi level position [24]; as such depending on the experimental conditions, there is a balance between Li_{Zn} and Li_i configurations in ZnO [25].

In the present paper, we demonstrate how Li behavior can be used for monitoring the migration and trapping of Zn_i during post-implantation anneals in ZnO single crystals. In particular, B-related defects act as an efficient source of Zn_i during annealing, while the presence of F dramatically reduces the injection of Zn_i into the crystal bulk and leads to their trapping and stabilization.

2. Experimental

Hydrothermally grown wurtzite ZnO single crystals purchased from Mineral Ltd. were used in the present study. In the virgin samples the Li content was found to be in the range of $\sim 2 \times 10^{17} \text{ cm}^{-3}$ homogeneously distributed throughout the wafers of 500 μm thick. The implants with B^+ and BF_2^+ ions were performed at room temperature at 7° off the [0001] direction to reduce channeling. In order to make defect generation profiles comparable, the implantations were performed

with the same energy per atomic mass unit (3.2 keV/amu), resulting in energies of 35 keV and 155 keV for B^+ and BF_2^+ , respectively. According to the SRIM code simulations [26] the projected range (R_p) of the implanted ions and the depth of the maximum of nuclear energy loss profile (R_{pd}) are ≈ 90 and ≈ 55 nm, respectively. In its turn, the doses were normalized according to the same total amount of primary defects as estimated by SRIM code simulations [26] giving $1.5 \times 10^{16} \text{ B cm}^{-2}$ and $3 \times 10^{15} \text{ BF}_2 \text{ cm}^{-2}$. In addition, a control sample was implanted with B^+ ions to the same dose as that with BF_2^+ ions, i.e. $3 \times 10^{15} \text{ B cm}^{-2}$. The anneals were performed in air at 500 °C–900 °C for 30 min using a standard tube furnace or using rapid thermal processing chamber (RTP) at 800 °C for 5 s.

The crystalline quality of the implanted samples before and after annealing was analyzed using Rutherford backscattering spectrometry in channeling mode (RBS/C) with 2 MeV $^4\text{He}^+$ ions incident along the [0001] direction and backscattered into a detector positioned at 100° relative to the incident beam direction. The RBS/C data were analyzed using one of the conventional algorithms [27] to deduce an effective number of scattering centers in the Zn sublattice, referred to below as ‘relative disorder’. The concentration versus depth profiles of Li, B and F were measured by secondary ion mass spectrometry (SIMS) using a Cameca IMS 7f microanalyzer with 10 keV O_2^+ or 15 keV Cs^+ ions as primary beam for the analysis of Li/B and F, respectively. The intensity-concentration calibration was performed using as-implanted samples as references. The depth conversion of the profiles was performed by measuring the sputtered crater depth using a Dektak 8 stylus profilometer and assuming a constant erosion rate.

3. Results and discussion

The disorder evolution in the course of post-implantation anneals in the samples implanted with B ions to an ion dose of $1.5 \times 10^{16} \text{ cm}^{-2}$ is illustrated by figure 1(a) showing defect-depth profiles on Zn sublattice as deduced from RBS/C spectra. It can be seen that the damage distribution in the as-implanted sample has a maximum close to the R_p rather than to the R_{pd} and has a Gaussian shape resembling the SRIM predicted distribution of the implanted atoms as clearly seen in the figure where the depth profiles of generated vacancies and B atoms as predicted by the SRIM code simulations are shown by the solid and the dashed lines, respectively. The crystalline structure starts recovering already at 500 °C and ion-induced defects exhibit gradual annealing with increasing temperature. However, even after 900 °C, a substantial fraction of defects still persists and higher temperatures are needed for complete crystalline restoration. It should be noted that substantial defect annealing occurs within a short period of time as seen from the comparison of 5 s and 30 min anneal data at 800 °C in figure 1(a). Such behavior of ion-induced defects under RTP annealing is not surprising and previously was observed in ZnO implanted with Zn [28] and rare earth ions [29]. It was demonstrated also that transient processes of

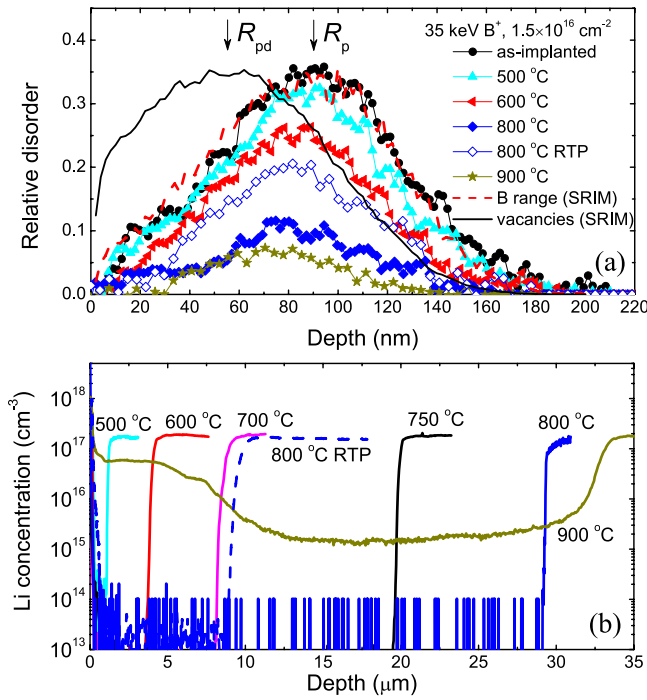


Figure 1. (a) Relative disorder in Zn sublattice as deduced from the RBS/C spectra and (b) corresponding Li concentration versus depth profiles as measured by SIMS in ZnO implanted with 35 keV B ions to $1.5 \times 10^{16} \text{ cm}^{-2}$ before and after annealing as indicated in the legends. The relative disorder and Li concentration versus depth profiles in the RTP annealed (800 °C for 5 s) sample are shown by the open symbols in (a) and the dashed line in (b). The profiles of the total vacancies and B atoms as predicted by SRIM code simulations are shown in (a) by the solid and the dashed line, respectively.

defect reconstruction and defect diffusion can occur supported by our results as shown below.

Figure 1(b) shows the Li concentration versus depth profiles in the annealed samples featuring a characteristic Li depletion region formed after annealing. Note that the as-implanted samples demonstrated the uniform Li distributions similar to those in the virgin samples (not shown). Such Li depleted region forms already at 500 °C and reaches $\sim 29 \mu\text{m}$ after the 800 °C 30 min anneal. Further annealing at 900 °C enhances the width of the Li depletion region up to $\sim 33 \mu\text{m}$, however, Li atoms start to diffuse back at this temperature. Previously, it has been argued that the formation of the Li depletion region (similar to that in figure 1(b)) is typical for implantations with Zn-substituting elements and ascribed to fast moving Li_i formed via the kick-out reaction ($\text{Zn}_i + \text{Li}_{\text{Zn}} \rightarrow \text{Zn}_{\text{Zn}} + \text{Li}_i$) where the Zn_i are emitted from the implanted region [19, 30]. In its turn, an excess of Zn_i needed for this reaction occurs due to preferential incorporation of implanted atoms on Zn sites. Therefore, the Li depleted region in figure 1(b) indicates that (i) B atoms reside preferentially on Zn sites and (ii) efficient injection of Zn_i occurs in a wide temperature range corroborating with the damage annealing kinetics shown in figure 1(a).

Furthermore, substantial injection of Zn_i occurs already during several first seconds following the trend for the disorder evolution as seen from the 800 °C profile in figure 1.

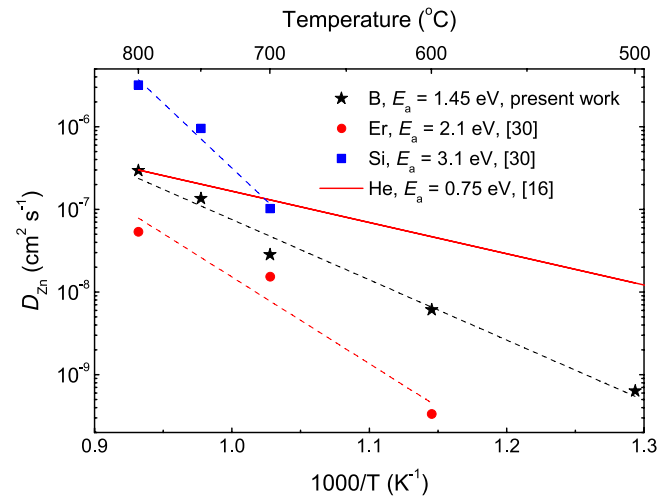


Figure 2. Arrhenius plot of the effective Zn_i diffusion obtained in the present work for B ions in comparison with those for Si and Er ions (the data are taken from [30]). Solid line depicts an extrapolated Zn_i diffusivity obtained for low temperature irradiation (see [16] for details).

This result corroborates well with previously reported Li redistribution in Zn implanted samples where outmost extension of the Li depletion region was reached after ~ 30 s anneals [31]. It was recently demonstrated that an effective diffusivity of Zn_i (D_{Zn}) can be estimated as a square of the width of the Li depleted region divided by the characteristic time equal to 30 s at each annealing temperature [30]. Following the methodology, figure 2 shows the Arrhenius plot for D_{Zn} as extracted from the Li depletion data in figure 1(b). The analysis reveals an activation energy of $\sim 1.45 \text{ eV}$ and pre-exponential factor of $1.5 \text{ cm}^2 \text{ s}^{-1}$. An extrapolated value of D_{Zn} obtained for low dose implantation performed at cryogenic temperature (40 K) [16] is also plotted in figure 2 for comparison. The difference in the E_a values obtained in [16] (0.75 eV) and the present work (1.45 eV) is not surprised. Indeed for low dose implants performed at cryogenic temperatures isolated defects are expected to form. In contrast, high dose implants performed at room temperature lead to the formation of more complex defect structures consisting of clusters of point defects as well as extended defects such as stacking faults and dislocation loops [32]. Taking in to account that a migration barrier for Zn_i predicted theoretically is $\sim 0.57 \text{ eV}$ [15] it may be concluded that the formation energy of Zn_i related to the dissociation of B ion-induced defect complexes should be in the range of $\sim 0.8\text{--}0.9 \text{ eV}$. Figure 2 also shows the data for Si and Er ions obtained with the same methodology as that used in the present paper [30]. The difference in the activation energies obtained for different implanted species (as indicated in the figure legend) is attributed to the different kinetics of the damage annealing for these elements. These difference can be attributed to the variations in atomic masses of the projectiles and, therefore, in the density of collision cascades generated, affecting the dominant defect type. However, the chemical nature of the implanted atoms can also play a substantial role that is also supported for B by practically identical shape/position of the damage depth profile and distribution of the

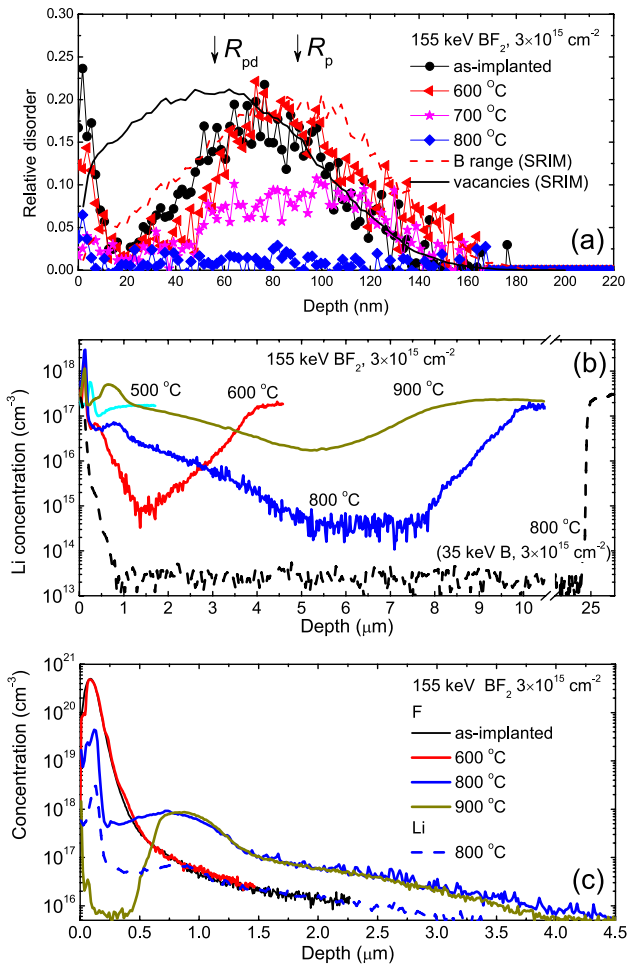


Figure 3. (a) Relative disorder as deduced from the RBS/C spectra and corresponding (b) Li and (c) F concentration versus depth profiles as measured by SIMS in ZnO implanted with 155 keV BF_2 ions to $3 \times 10^{15} \text{ cm}^{-2}$ before and after annealing as indicated in the legends. The Li concentration versus depth profiles in the sample implanted with 35 keV B ions to $3 \times 10^{15} \text{ cm}^{-2}$ and annealed at 800 °C is also shown by the dashed line in (b). The Li profile after 800 °C annealing is included for comparison (dashed line) in (c). The profiles of the total vacancies and B atoms as predicted by SRIM code simulations are shown in (a) by the solid and the dashed line, respectively.

implanted atoms (see figure 1(a)). Thus, our results indicate a dramatic role of the implanted atoms on the stability and annealing behavior of ion-induced defects in ZnO.

The effect of F atoms on the behavior of Zn_i is illustrated by figure 3 showing the disorder versus depth profiles (a) and the distributions of Li (b) and F (c) atoms in the BF_2 implanted samples subjected to the anneals as indicated in the legends. Note that despite B (figure 1(a)) and BF_2 (figure 3(a)) implants should produce the same amount of defects according to the SRIM code simulations [26], the measured amount of damage is considerably higher for the B implantation. This effect is attributed to the domination of dopant-defect reactions for B, as discussed in details elsewhere [32]. Although the disorder annealing kinetics at 600 °C–800 °C for BF_2 reveals similar

trends as those for B ions, the Li redistribution exhibits very different behavior (figure 3(b)). Indeed, the Li depletion is not as strong as that for B and it is not exceeding $10 \mu\text{m}$ after 800 °C. Moreover, both the front and the back slopes of the Li depleted region are not sharp and Li piles-up in the end-of-range region ($\sim 1 \mu\text{m}$) for 800 and 900 °C anneals. Such Li behavior can not be attributed simply to the lower B dose as compared to figure 1, since the control sample implanted with B ions to the same dose as BF_2 one ($3 \times 10^{15} \text{ cm}^{-2}$) demonstrated a wide Li depletion reaching $25 \mu\text{m}$ (see the dashed line in figure 3(b)). Therefore, the remaining candidate to make the difference is F.

The F implantation profile is stable up to 600 °C, while further annealing leads to a dramatic redistribution and loss of F atoms (figure 3(c)). In particular, upon the 800 °C anneal, F atoms diffuse in to the bulk and pileup at the end-of-range region, i.e. at $\sim 1 \mu\text{m}$, accompanied with a dramatic loss of F atoms from the implanted peak. Further annealing at 900 °C leads to complete removal of F atoms around R_p and formation of F lean region, while the diffusion tail and the F pileup remain practically unchanged as compared to the 800 °C anneal. Note that F substituting oxygen (F_O) is a donor and it has been shown previously that the deactivation of F atoms is accompanied by strong retardation of Zn self-diffusion [14]. To explain this effect it has been proposed that formation of acceptor-like complexes involving V_{Zn} , such as $\text{F}_O\text{-V}_{\text{Zn}}$, can play a role reducing the concentration of free V_{Zn} 's, otherwise mediating Zn self-diffusion [14]. A similar scenario can be put forward to explain a lower extend of the Li depletion in BF_2 implanted samples as compared to that for the B implants. Indeed, a large concentration of $\text{F}_O\text{-V}_{\text{Zn}}$ complexes can act as an efficient barrier or better to say a trap for the migrating Zn_i released from the implanted region during annealing. In addition, figure 3(c) shows also that Li profile after 800 °C annealing has a similar shape as that for F. This may indicate a strong interaction between Li and F atoms where trapping of Li atoms may potentially occur via the formation of $\text{F}_O\text{-Li}_{\text{Zn}}$ ($\text{F}_O\text{-2Li}_{\text{Zn}}$) complexes [33, 34].

4. Conclusions

In conclusion, the behavior of Zn_i during annealing in B/ BF_2 implanted samples has been studied by a combination of structural/diffusion analysis, in particular using residual impurity Li as a tracer. Damage annealing exhibits single stage behavior and B-induced disorder region acts as an efficient source for Zn_i at 500 °C–900 °C. Migration of Zn_i in the B-implanted samples occurs with an activation energy of 1.45 eV. In its turn, the migration of Zn interstitials is strongly suppressed in the BF_2 implanted samples and it was argued that Zn_i may be trapped by defect complexes related to the presence of F, e.g. $\text{F}_O\text{-V}_{\text{Zn}}$. As a result, we showed that monitoring the Li depleted region in ion implanted ZnO may indeed be used for extracting Zn_i energetics, however the process may be affected by additional defect reactions to be taken into account.

Acknowledgments

Financial support was kindly provided by the Research Council of Norway and University of Oslo through the frontier research project FUNDAMeNT (project number 251131, Fri-Pro ToppForsk-program).

ORCID iDs

Alexander Azarov  <https://orcid.org/0000-0003-0602-9624>

References

- [1] Pearton S J, Norton D P, Ip K, Heo Y W and Steiner T 2005 Recent progress in processing and properties of ZnO *Prog. Mater. Sci.* **50** 293–340
- [2] Avrutin V, Silversmith D J and Morkoç H 2010 Ferromagnetism in ZnO- and GaN-based diluted magnetic semiconductors: achievements and challenges *Proc. IEEE* **98** 1288–301
- [3] Özgür Ü, Alivov Y I, Liu C, Teke A, Reshchikov M A, Doğan S, Avrutin V, Cho S-J and Morkoç H 2005 A comprehensive review of ZnO materials and devices *J. Appl. Phys.* **98** 041301
- [4] Look D C, Farlow G C, Reunchan P, Limpijumnong S, Zhang S B and Nordlund K 2005 Evidence for native-defect donors in *n*-type ZnO *Phys. Rev. Lett.* **95** 225502
- [5] Park C H, Zhang S B and Wei S-H 2002 Origin of *p*-type doping difficulty in ZnO: The impurity perspective *Phys. Rev. B* **66** 073202
- [6] Zhang S B 2002 The microscopic origin of the doping limits in semiconductors and wide-gap materials and recent developments in overcoming these limits: a review *J. Phys.: Condens. Matter* **14** R881
- [7] Petretto G and Bruneval F 2014 Comprehensive *ab initio* study of doping in bulk ZnO with group-V elements *Phys. Rev. Appl.* **1** 024005
- [8] Xiu F X, Yang Z, Mandalapu L J, Zhao D T, Liu J L and Beyermann W P 2005 High-mobility Sb-doped *p*-type ZnO by molecular-beam epitaxy *Appl. Phys. Lett.* **87** 152101
- [9] Fan J C, Sreekanth K M, Xie Z, Chang S L and Rao K V 2013 *p*-Type ZnO materials: theory, growth, properties and devices *Prog. Mater. Sci.* **58** 874–985
- [10] Braunstein G, Muraviev A, Saxena H, Dhare N, Richter V and Kalish R 2005 *p* type doping of zinc oxide by arsenic ion implantation *Appl. Phys. Lett.* **87** 192103
- [11] Myers M A, Myers M T, General M J, Lee J H, Shao L and Wang H 2012 *p*-type ZnO thin films achieved by N⁺ ion implantation through dynamic annealing process *Appl. Phys. Lett.* **101** 112101
- [12] Look C, Leedy K D, Vines L, Svensson B G, Zubiaga A, Tuomisto F, Doust D R and Brillson L J 2011 Self-compensation in semiconductors: the Zn vacancy in Ga-doped ZnO *Phys. Rev. B* **84** 115202
- [13] Tomlins G W, Routbort J L and Mason T O 2000 Zinc self-diffusion, electrical properties, and defect structure of undoped, single crystal zinc oxide *J. Appl. Phys.* **87** 117–23
- [14] Azarov A, Venkatachalapathy V, Mei Z, Liu L, Du X, Galeckas A, Monakhov E, Svensson B G and Kuznetsov A 2016 Self-diffusion measurements in isotopic heterostructures of undoped and *in situ* doped ZnO: zinc vacancy energetics *Phys. Rev. B* **94** 195208
- [15] Janotti A and Van de Walle C G 2009 Fundamentals of zinc oxide as a semiconductor *Rep. Prog. Phys.* **72** 126501
- [16] Bhoondoo C, Hupfer A, Vines L, Monakhov E V and Svensson B G 2016 Evolution kinetics of elementary point defects in ZnO implanted with low fluences of helium at cryogenic temperature *Phys. Rev. B* **94** 205204
- [17] Vlasenko L S and Watkins G D 2005 Optical detection of electron paramagnetic resonance for intrinsic defects produced in ZnO by 2.5 MeV electron irradiation *in situ* at 4.2 K *Phys. Rev. B* **72** 035203
- [18] Shao L, Liu J, Chen Q Y and Chu W-K 2003 Boron diffusion in silicon: the anomalies and control by point defect engineering *Mater. Sci. Eng. R* **42** 65–114
- [19] Azarov A Y, Neuvonen P T, Knutsen K E, Vines L, Svensson B G and Kuznetsov A Y 2013 Impurity sublattice localization in ZnO revealed by Li marker diffusion *Phys. Rev. Lett.* **110** 175503
- [20] Lu J G *et al* 2006 Control of *p*- and *n*-type conductivities in Li-doped ZnO thin films *Appl. Phys. Lett.* **89** 112113
- [21] Zeng Y J, Ye Z Z, Lu J G, Xu W Z, Zhu L P, Zhao B H and Limpijumnong S 2006 Identification of acceptor states in Li-doped *p*-type ZnO thin films *Appl. Phys. Lett.* **89** 042106
- [22] Polarz S *et al* 2009 A Systematic study on zinc oxide materials containing group I metals (Li, Na, K)-synthesis from organometallic precursors, characterization, and properties *Chem. Mater.* **21** 3889–97
- [23] Wardle M G, Goss J P and Briddon P R 2005 Theory of Li in ZnO: a limitation for Li-based *p*-type doping *Phys. Rev. B* **71** 155205
- [24] Carvalho A, Alkauskas A, Pasquarello A, Tagantsev A K and Setter N 2009 A hybrid density functional study of lithium in ZnO: Stability, ionization levels, and diffusion *Phys. Rev. B* **80** 195205
- [25] Knutsen K E, Johansen K M, Neuvonen P T, Svensson B G and Kuznetsov A Y 2013 Diffusion and configuration of Li in ZnO, *J. Appl. Phys.* **113** 023702
- [26] Ziegler J F, Biersack J P and Littmark U 1985 *The Stopping and Range of Ions in Solids* vol 1 (New York: Pergamon) p 321
- [27] Schmid K 1973 Some new aspects for the evaluation of disorder profiles in silicon by backscattering *Radiat. Eff.* **17** 201–7
- [28] Chan K S, Vines L, Li L, Jagadish C, Svensson B G and Wong-Leung J 2016 Zn precipitation and Li depletion in Zn implanted ZnO *Appl. Phys. Lett.* **109** 022102
- [29] Miranda S M C, Peres M, Monteiro T, Alves E, Sun H D, Gerschke T, Vianden R and Lorenz K 2011 Rapid thermal annealing of rare earth implanted ZnO epitaxial layers *Opt. Mater.* **33** 1139–42
- [30] Azarov A, Aarseth B L, Vines L, Hallén A, Monakhov E and Kuznetsov A 2019 Defect annealing kinetics in ZnO implanted with Zn substituting elements: Zn interstitials and Li redistribution *J. Appl. Phys.* **125** 075703
- [31] Neuvonen P T, Vines L, Svensson B G and Kuznetsov A Y 2013 Intrinsic point-defect balance in self-ion-implanted ZnO *Phys. Rev. Lett.* **110** 015501
- [32] Azarov A Y, Wendler E, Kuznetsov A Y and Svensson B G 2014 Crucial role of implanted atoms on dynamic defect annealing in ZnO *Appl. Phys. Lett.* **104** 052101
- [33] Chen L, Xiong Z, Wan Q and Li D 2011 Suppression of the formation of interstitial Li through (F, Li) codoping ZnO *J. Phys.: Conf. Ser.* **276** 012158
- [34] Yamamoto T and Katayama-Yoshida H 2000 Unipolarity of ZnO with a wide-band gap and its solution using codoping method *J. Cryst. Growth* **214/215** 552–5